

---

# How Much Is One Recurrence Worth? Iso-Depth Scaling Laws for Looped Language Models

---

Kristian Schwethelm<sup>1</sup>Daniel Rückert<sup>1,2,3</sup>Georgios Kaissis<sup>4</sup>

<sup>1</sup>Chair for AI in Healthcare and Medicine,  
Technical University of Munich (TUM) and TUM University Hospital, Germany

<sup>2</sup>Department of Computing, Imperial College London, UK

<sup>3</sup>Munich Center for Machine Learning (MCML), Germany

<sup>4</sup>Hasso Plattner Institute for Digital Engineering, University of Potsdam, Germany

## Abstract

We measure how much one extra recurrence is worth to a looped (depth-recurrent) language model, in equivalent unique parameters. From an iso-depth sweep of 116 pretraining runs across recurrence counts  $r \in \{1, 2, 4, 8\}$  spanning  $\sim 50\times$  in training compute, we fit a joint scaling law  $L = E + A(N_{\text{once}} + r^\varphi N_{\text{rec}})^{-\alpha} + B D^{-\beta}$  and recover a new *recurrence-equivalence exponent*  $\varphi = 0.46$  at  $R^2 = 0.997$ . Intuitively,  $\varphi$  tells us whether looping a block  $r$  times is equivalent in validation loss to  $r$  unique blocks of a non-looped model (full equivalence,  $\varphi=1$ ) or to a single block run repeatedly with no capacity gain ( $\varphi=0$ ). Our  $\varphi = 0.46$  sits in between, so each additional recurrence predictably increases validation loss at matched training compute. For example, at  $r=4$  a 410M looped model performs on par with a 580M non-looped model, but pays the training cost of a 1B non-looped one. On a five-axis downstream evaluation, the gap persists on parametric-knowledge tasks and closes on simple open-book tasks, while reasoning tasks are not resolvable at our compute budgets. For any looped LM, our  $\varphi$  converts the design choice of  $r$  into a predictable validation-loss cost, and future training recipes and architectures can be compared by how much they raise  $\varphi$  above 0.46.

## 1 Introduction

Can a transformer block looped  $r$  times replace  $r$  non-looped blocks at matched compute? Looped, or depth-recurrent, transformers iterate a shared block of layers multiple times [1]. The looped architecture decouples unique parameter count from effective depth at fixed per-token inference FLOPs, and introduces an inductive bias toward reasoning [2]. These properties have motivated a recent wave of work on looped language models [3–9]. However, in practice, most looped LMs use only small recurrence counts [4–6], revealing a cost: a shared block reused  $r$  times may not fully substitute for  $r$  unique blocks at matched FLOPs. How many unique parameters one extra recurrence is worth has not been measured directly. Concurrent scaling-law work fixes the unique parameter count and lets effective depth and per-token inference FLOPs grow with  $r$  [9]. Their setup traces the compute-optimal  $r$  at fixed parameter memory, but varies parameter sharing, effective depth, and inference cost, so any scaling exponent fit this way cannot separate them.

To isolate parameter sharing from effective depth, we run an iso-depth sweep across four prelude-recur-coda architectures with recurrence count  $r \in \{1, 2, 4, 8\}$ , where  $r=1$  is the non-looped baseline (see schematic in Appendix B, Figure 5). We sweep six compute budgets from  $4.64 \times 10^{17}$  to  $2.15 \times 10^{19}$  FLOPs ( $\sim 50\times$ ) to find the compute-optimum per architecture, yielding 116 pretraining runs. The four variants execute the same number of forward layers per token and, at matched width,

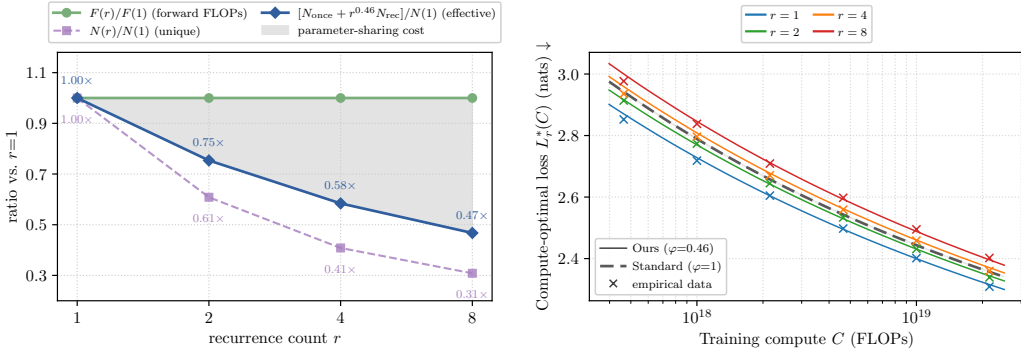


Figure 1: **How much is one recurrence worth?** *Left:* at matched effective depth, per-token forward FLOPs  $F(r)$  stay flat while unique parameters  $N(r)$  drop as  $r$  grows. Effective parameters  $N_{\text{once}} + r^\varphi N_{\text{rec}}$  under the fitted  $\varphi=0.46$  (blue diamonds) drop more slowly. The shaded gap illustrates the parameter-sharing cost in parameter-equivalent terms. *Right:* compute-optimal validation-loss frontier  $L_r^*(C)$ . Empirical per-budget optima (crosses) track our  $\varphi=0.46$  fit (solid, one curve per  $r$ ). The standard form ( $\varphi=1$ ) collapses all four architectures onto a single frontier (dashed), which fits none of the empirical results.

incur the same per-token training and inference FLOPs. Yet unique non-embedding parameters drop by  $3.2\times$  as  $r$  grows (Figure 1, left), the source of the *parameter-sharing cost* we quantify.

Using our iso-depth sweep, we first fit standard Chinchilla laws [10] separately per architecture to assess their scaling behaviour. We find that models with higher recurrence count  $r$  prefer wider widths and fewer training tokens per parameter. However, their wider widths raise the per-token compute cost, so at matched compute the looped optimum trains on fewer total tokens than the non-looped optimum. The per-architecture fits give optimal training settings for each  $r$ , but they do not answer how much one recurrence is worth. Comparing the four fitted scaling exponents across  $r$  is also misleading, because  $r$  does not enter the scaling law.

We propose a joint scaling law  $L(N_{\text{once}}, N_{\text{rec}}, D, r) = E + A(N_{\text{once}} + r^\varphi N_{\text{rec}})^{-\alpha} + B D^{-\beta}$  with a new *recurrence-equivalence exponent*  $\varphi$ . Here  $N_{\text{once}} + N_{\text{rec}} = N$  splits the total unique parameters into the shared recurrent block ( $N_{\text{rec}}$ ) and the single-use prelude and coda ( $N_{\text{once}}$ ). Fully-looped models are recovered by  $N_{\text{once}} = 0$ . With  $\varphi$  shared across architectures, one fit describes all 116 runs instead of four separate Chinchilla laws. Additionally,  $\varphi$  has two natural reference points.  $\varphi = 1$  attributes full parameter equivalence to each recurrence (no sharing cost), so the looped model matches the non-looped baseline’s validation loss.  $\varphi = 0$  attributes none (a pure sharing cost). We find  $\varphi = 0.46$  with  $R^2 = 0.997$ , between the two (see Figure 1, left). Figure 1 (right) shows the compute-optimal frontier landing on our free- $\varphi$  fit and away from  $\varphi=1$ . Under  $\varphi=1$ , all four architectures would reach the same validation loss, which our data rule out. Specifically, at  $r=4$  and matched training FLOPs, the looped model reaches only the validation loss of a non-looped model that has 42% fewer parameters. For example, a 410M  $r=4$  model performs on par with a 580M non-looped model, but incurs the training cost of a 1B non-looped model.

Our five-axis downstream evaluation confirms this picture.  $\varphi = 0.46$  predicts the gap directly on parametric-knowledge tasks, open-book tasks close as validation loss decreases, and reasoning axes remain below measurement noise at our compute budgets, making the validation-loss gap the most measurable target for looped LM research at development scale.

## Contributions.

1. **Joint scaling law.** We fit a joint scaling law relating validation loss  $L$  to unique parameters  $N$ , training tokens  $D$ , and recurrence count  $r$  via a single *recurrence-equivalence exponent*  $\varphi$ . The formulation applies to any looped transformer. For the prelude-recur-coda architecture we find  $\varphi = 0.46$ , a single-number benchmark against which improved training recipes and new looped LM designs can be measured.

2. **Scaling behaviour of looped LMs.** Our iso-compute sweep at matched effective depth is the first for looped LMs. The per-architecture Chinchilla fits show looped variants prefer wider widths with fewer total training tokens than the non-looped optimum, giving concrete allocation starting points for future looped LM training runs.
3. **Downstream evaluation suite.** We construct a five-axis evaluation suite, revealing where the parameter-sharing cost shows up across downstream capabilities. Validation loss is a reliable target at development scale, while signal from downstream reasoning tasks remains weak.

## 2 Related Work

**Looped language models.** The Universal Transformer [1] introduced weight sharing across depth. Such looped language models have recently drawn renewed attention as a route to implicit, latent-space reasoning and test-time compute scaling, where iterating a shared block lets a model spend more compute per token. Huggins [3] and Ouro [4] have scaled the paradigm to  $\sim 3$ B parameters and trillion-token training budgets with strong downstream results, often matching much larger dense transformers. However, test-time compute from looping comes at a proportional training-compute cost. Another line of work [2] runs compute-matched comparisons at single training budgets and reports a consistent pattern: looped models trail non-looped baselines on validation loss and parametric-knowledge tasks but close the gap or outperform them on reasoning benchmarks. We extend these findings to the scaling-law setting [10]. Unlike per-architecture scaling law fits, our joint law fits all architectures together under a single recurrence-equivalence exponent  $\varphi$ . Architectural and training-efficiency methods like retrofitting [7, 8], adaptive compute [5, 6], and truncated backpropagation [3, 9] reduce the per-step training-FLOPs cost of a looped step and could increase  $\varphi$ . We study the established prelude-recur-coda architecture [3] and leave testing other recipes to future work. See Appendix A for extended discussion.

**Iso-parameter scaling laws.** Concurrent work by Prairie et al. [9] fits a iso-parameter scaling law at fixed unique parameter count  $N$ , motivated by equal parameter memory footprint between architectures. However, in contrast to our setup, depth, per-token inference FLOPs, and KV cache memory all grow with the recurrence count. The two setups therefore answer different questions: Prairie et al. [9] trace the compute-optimal recurrence count at fixed parameter memory, we measure the per-recurrence sharing cost at fixed effective depth. See Appendix A for a detailed comparison.

## 3 Methodology

We compare four transformer variants: a non-looped baseline ( $r=1$ ) and looped models with  $r \in \{2, 4, 8\}$  recurrences, all with 20 effective layers. At matched model width, per-token training and inference FLOPs match across  $r$  up to a small correction for an input-injection layer. At every compute budget, all four architectures consume the same total training FLOPs.

### 3.1 Looped Transformer Architecture

All four variants follow the prelude-recur-coda template [3], with effective depth obtained as

$$L_{\text{eff}} = n_{\text{prelude}} + r \cdot n_{\text{recur}} + n_{\text{coda}} = 20. \quad (1)$$

We fix  $(n_{\text{prelude}}, n_{\text{coda}}) = (2, 2)$  and use a shared recurrent block of  $n_{\text{recur}} = 16/r$  layers executed  $r$  times, giving  $(8, 4, 2)$  recurrent layers for  $r \in \{2, 4, 8\}$ . Width is parameterised as  $d_{\text{model}} = 64s$  for an integer scale factor  $s$ , with attention head dimension 128.

Following Geiping et al. [3], we employ a linear input-injection layer, which they found important at scale. An ablation (Appendix B.2) confirms this. Linear injection matches additive residual injection and outperforms the no-injection variant. Its small FLOPs overhead is included in every iso-FLOPs comparison. Full architectural details are in Appendix B.

### 3.2 FLOPs Accounting Under Parameter Sharing

Let  $n_b = 12d^2$  be the non-embedding parameter count of a transformer block at width  $d$  (four  $d \times d$  attention projections plus the  $d \rightarrow 4d \rightarrow d$  MLP), and  $n_i = 2d^2$  the injection-layer count. We follow the standard  $2N$  and  $6N$  convention for per-token forward and training FLOPs with  $N$  non-embedding parameters [11, 10].

Our looped transformer executes the prelude once, the recur block  $r$  times (each preceded by the injection layer), and the coda once. Per-token forward FLOPs are therefore

$$F_{\text{fwd}}(r) = 2[(n_{\text{prelude}} + r \cdot n_{\text{recur}} + n_{\text{coda}})n_b + r \cdot n_i] = 2L_{\text{eff}}n_b + 2r \cdot n_i \approx F_{\text{fwd}}(1), \quad (2)$$

where  $L_{\text{eff}} = n_{\text{prelude}} + r \cdot n_{\text{recur}} + n_{\text{coda}} = 20$  is fixed by design. All looped and non-looped variants therefore see the same  $F_{\text{fwd}}$  up to an injection overhead of  $r/120 \in \{1.7\%, 3.3\%, 6.7\%\}$  at  $r \in \{2, 4, 8\}$ . Under full backpropagation, training FLOPs are  $F_{\text{train}}(r) = 3F_{\text{fwd}}(r)$ , so at a fixed compute budget  $C$  every variant trains on essentially the same token count  $D \approx C/F_{\text{train}}$ .

The parameter budget differs. Only the recur block is shared across recurrences, so the unique non-embedding parameter count

$$N(r) = (n_{\text{prelude}} + n_{\text{recur}} + n_{\text{coda}})n_b + n_i, \quad (3)$$

counts  $n_{\text{recur}}$  once rather than  $r$  times. At fixed  $L_{\text{eff}}$ ,  $N(r)$  therefore shrinks by  $\sim 3.2\times$  over our grid: at  $s=10$ ,  $N \in \{98.3, 59.8, 40.2, 30.3\}$  M for  $r \in \{1, 2, 4, 8\}$ .

In summary, the four variants match on per-token inference and training FLOPs. The key difference is on the parameter side: looped variants have substantially fewer unique parameters. This may reduce their capacity to store knowledge, but also cuts weight and optimiser-state memory, per-step update cost, and wall-clock training time.

### 3.3 Joint Scaling Law

Through the Chinchilla lens  $L(N, D) = E + AN^{-\alpha} + BD^{-\beta}$ , our iso-compute design holds  $D$  fixed across  $r$  but reduces  $N$ . Here  $L$  is validation loss (nats),  $N$  is the non-embedding parameter count,  $D$  is training tokens,  $E$  is the irreducible loss floor, and  $A, B, \alpha, \beta$  are fitted constants. The training-FLOPs spend per unique parameter

$$\rho(r) = \frac{F_{\text{train}}(r) \cdot D}{N(r)} \approx \frac{C}{N(r)} \quad (4)$$

grows roughly linearly with  $r$ . The same compute is spread over fewer parameters. Whether the loss responds to this extra spend at the Chinchilla rate or a slower one is the question we study.

Within the prelude-recur-coda architecture, the recurrent block is shared across its  $r$  executions, while the prelude and coda execute once per token. We therefore split the unique non-embedding parameter count into an executed-once component and a shared recurrent component,

$$N_{\text{once}} = (n_{\text{prelude}} + n_{\text{coda}})n_b + n_i, \quad N_{\text{rec}} = n_{\text{recur}}n_b, \quad (5)$$

so that  $N = N_{\text{once}} + N_{\text{rec}}$  at every  $(r, s)$  on our grid. Note that fully-looped architectures can be recovered by  $N_{\text{once}} = 0$ .

With this split in place, we extend the Chinchilla form with a *recurrence-equivalence exponent*  $\varphi \in \mathbb{R}$  on the shared component only:

$$L(N_{\text{once}}, N_{\text{rec}}, D, r) = E + A(N_{\text{once}} + r^\varphi N_{\text{rec}})^{-\alpha} + BD^{-\beta}. \quad (6)$$

Two reference points are informative.  $\varphi = 0$  corresponds to a pure sharing cost: extra recurrences yield no improvement and  $r$  is invisible to the law.  $\varphi = 1$  corresponds to the fully-unrolled non-looped model at matched effective depth: each recurrence contributes as much as an unshared block,

so all four architectures would perform the same. Values  $0 < \varphi < 1$  quantify partial recovery.  $\varphi > 1$  would mean each recurrence contributes more than an unshared block, so looped models would outperform the non-looped baseline at matched effective depth. We fit Equation 6 across all 116 runs in Section 4.3.

## 4 Iso-Depth Scaling Laws

We train each of the four architectures at six compute budgets,  $C \in \{4.64 \times 10^{17}, 10^{18}, 2.15 \times 10^{18}, 4.64 \times 10^{18}, 10^{19}, 2.15 \times 10^{19}\}$  FLOPs, spanning  $\sim 50\times$ . At each budget we sweep model width to find the compute-optimal point. The per-budget grid is in Appendix D.

### 4.1 Experimental Details

**Implementation.** Our implementation builds on nanochat [12]: a decoder-only transformer with RMSNorm [13], RoPE [14], QK normalisation [15], and squared-ReLU MLPs [16]. We use FlashAttention-2 & 3 [17, 18] as the attention backends.

**Optimisation.** Matrix parameters are optimised with MuonH [19, 20]. Embedding, unembedding, and norm parameters are optimised with AdamW [21]. Weight decay is set to zero (a first-order no-op under MuonH’s Frobenius-sphere constraint [22]). Hyperparameters transfer across width and training horizon via the HyperP framework [22] with reference width  $d_{\text{ref}}=640$  ( $s=10$ ). In Appendix C, we sweep base LR and batch size at the reference width and find optima agreeing across architectures (LR regret below 0.005 nats per architecture). All runs use base LR  $\eta_{\text{base}} = 0.014$  and batch size  $B = 262,144$  tokens, with the LR linearly decayed to 10% of its peak.

**Data and validation.** Training data is a subset of FineWeb-Edu [23], tokenised with the Llama 2 tokenizer [24] (32K vocabulary) and pre-packed into fixed-length sequences of 2,049 tokens. Thus, all four architectures see exactly the same data stream. Validation loss is reported in nats on a held-out FineWeb-Edu split packed identically to training.

### 4.2 Per-Architecture Chinchilla Fits

Figure 2 shows validation loss against unique non-embedding parameters  $N$  at our (budget, architecture) grid. At fixed compute  $C$  all four architectures trace an iso-FLOPs parabola in  $\log N$ . The parabolas are systematically offset upward and flatter for larger  $r$ , with looped minima at *wider* widths than the non-looped baseline. We summarise this surface by fitting the Chinchilla-style parametric scaling law

$$L(N, D) = E + AN^{-\alpha} + BD^{-\beta} \tag{7}$$

separately for each architecture.

**Fitting protocol.** We follow Hoffmann et al. [10] and minimise the Huber loss [25] ( $\delta = 10^{-3}$ ) between predicted and empirical *log* validation loss using L-BFGS [26]. Specifically, we parameterise the law in log-space ( $a = \log A$ ,  $b = \log B$ ,  $e = \log E$ ) and minimise

$$\mathcal{L}(a, \alpha, b, \beta, e) = \sum_i \text{Huber}_\delta(\text{LSE}(a - \alpha \log N_i, b - \beta \log D_i, e) - \log L_i), \tag{8}$$

where LSE is log-sum-exp. The log-space objective treats relative errors uniformly across the wide dynamic range of  $N$  and  $D$ . Because the objective is non-convex, we take the best of 500 random L-BFGS-B restarts with parameters constrained to the box  $a, b \in [-5, 35]$ ,  $\alpha, \beta \in [0, 2.5]$ ,  $e \in [-3, 2]$  and starting points drawn uniformly within it (up to 10,000 iterations each).

**Fitted parameters.** Table 1 reports the fitted parameters per architecture. All four fits achieve  $R^2 > 0.997$  (predicted-vs-actual scatter and residuals in Appendix E).

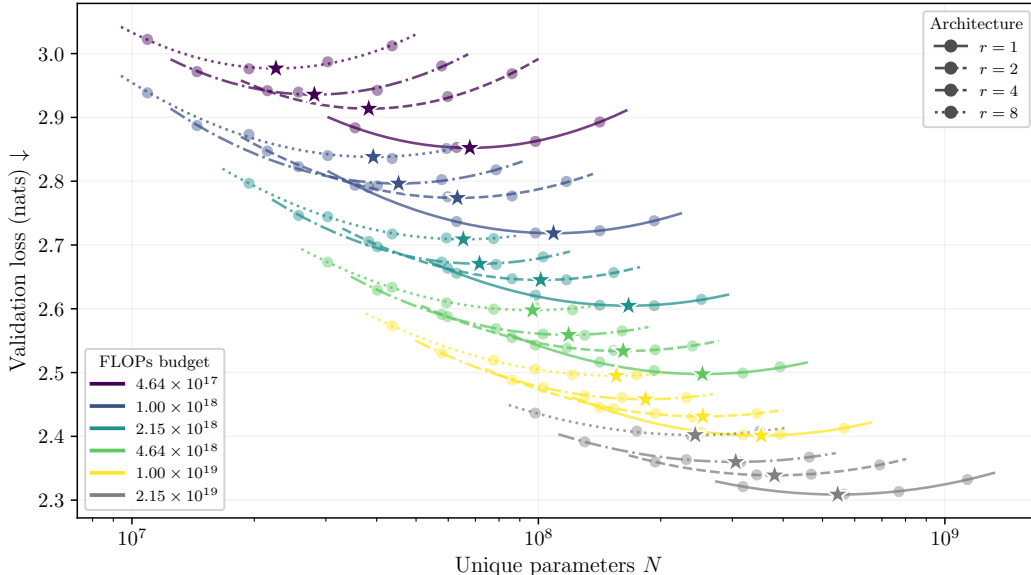


Figure 2: Scaling curves at fixed compute budgets. Validation loss vs. unique non-embedding parameters  $N$  at six training compute budgets (color). Recurrence  $r \in \{1, 2, 4, 8\}$  is distinguished by linestyle. Thin curves are per-(budget,  $r$ ) parabolic fits in  $\log N$ . Stars mark the fitted compute-optimal  $(N^*, L^*)$  points.

Table 1: Chinchilla scaling-law fit parameters per architecture. Huber loss is the objective at the optimum (Equation 8).  $R^2$  is on raw nats. Amplitudes  $A, B$  are rounded to 2 significant figures because they are only loosely identified under iso-compute designs [27].

Arch.	$A$	$\alpha$	$B$	$\beta$	$E$	Huber ( $\times 10^{-5}$ )	$R^2$
$r=1$	58	0.251	150	0.267	1.56	5.84	0.9979
$r=2$	33	0.216	910	0.365	1.60	5.27	0.9983
$r=4$	23	0.191	1300	0.388	1.56	6.81	0.9976
$r=8$	41	0.235	780	0.362	1.69	5.33	0.9980

**Exponent comparison.** At matched compute, looped variants scale toward more tokens per unique parameter than the non-looped baseline. The Chinchilla-optimal data-scaling exponent  $a_D = \beta/(\alpha + \beta)$  lands at  $[0.61, 0.67]$  across  $r \in \{2, 4, 8\}$  versus 0.52 for  $r=1$ , with parameter exponents  $\alpha$  similar across architectures (clustered in 0.19–0.25). As noted in Section 1, the per-architecture exponents sit on different compute-optimal trajectories and are not directly comparable.

**Compute-optimal allocation and gap.** Unlike the exponents, the compute-optimal loss frontier  $L_r^*(C)$  is directly comparable across  $r$ . We derive the optimal parameter and token allocation  $N^*(C), D^*(C)$  by minimising  $L(N, C/F(N))$  over  $N$  at each budget  $C$ , with  $F(N)$  the architecture’s empirical per-token FLOPs at  $N$ . The optimal *width*  $s^*$  is larger for higher  $r$ , while the optimal unique parameter count  $N^*$  is smaller (Figure 3, left). Sharing reduces parameters by up to  $\sim 3.2\times$  across our grid, which the optimum compensates for by widening. The wider  $s^*$  raises per-token FLOPs, so at matched  $C$  the optimal training tokens  $D^*$  are correspondingly smaller for higher  $r$  (Figure 3, right). The resulting loss frontier trails the baseline by  $[0.03, 0.06]$  nats at  $r=2$ ,  $[0.05, 0.08]$  nats at  $r=4$ , and  $[0.09, 0.12]$  nats at  $r=8$  across the six budgets, growing monotonically with  $r$ . The gap increases at lower budgets but flattens at our largest: between  $10^{19}$  and  $2.15 \times 10^{19}$  FLOPs, the  $r=2$  and  $r=8$  gaps change by  $\leq 0.001$  nats and the  $r=4$  gap by 0.006 nats. Within our compute window, the data show no approach toward a crossover, where a looped model would outperform the baseline.

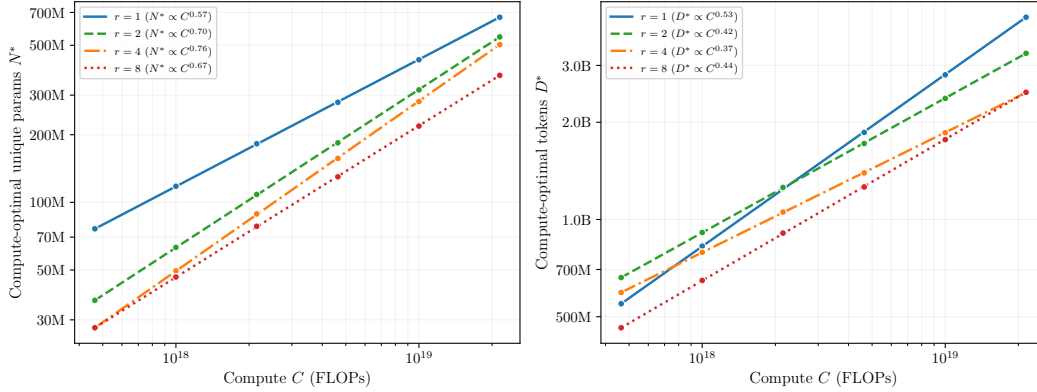


Figure 3: Compute-optimal allocation per architecture. Left: optimal unique parameter count  $N^*(C)$  with fitted exponent in the legend. Right: optimal training tokens  $D^*(C)$ .

Table 2: Joint  $(N_{\text{once}}, N_{\text{rec}}, D, r)$  scaling law (Equation 6) fit. The free- $\varphi$  row reports 95% block-bootstrap CIs (200 resamples of (budget, architecture) cells) below the  $\varphi$  point estimate. Amplitudes  $A, B$  are only loosely identified under iso-compute designs [27] and are omitted from the table.

Form	$\alpha$	$\beta$	$E$	$\varphi$	$R^2$
Joint, $\varphi$ free	0.199	0.369	1.57	0.459 [0.41, 0.53]	0.9972
Restricted ( $\varphi = 0$ , pure sharing cost)	0.227	0.390	1.71	0.00	0.9858
Restricted ( $\varphi = 1$ , fully-unrolled equivalence)	0.218	0.410	1.66	1.00	0.9552

### 4.3 Joint Scaling Law Fit

The four per-architecture fits above use 20 free parameters in total and, as noted, each summarises a different  $(N, D)$  region. We now fit the joint law introduced in Section 3.3 (Equation 6). A single recurrence-equivalence exponent  $\varphi$  shared across architectures reduces the degrees of freedom to six and places every architecture on a common  $(N_{\text{once}} + r^\varphi N_{\text{rec}}, D)$  surface.

**Fit and interpretation.** We minimise the same Huber-on-log objective as Equation 8, this time over six parameters  $(A, \alpha, B, \beta, E, \varphi)$  jointly across all 116 runs. Table 2 reports the result alongside the two restricted variants.

The fitted  $\varphi = 0.46$  sits well below the fully-unrolled reference point of 1. Each additional recurrence acts as if multiplying the shared-block contribution by only  $r^{0.46}$ , so at  $r=4$  the recur block contributes as if it were  $4^{0.46} \approx 1.86$  unshared blocks, not 4. The block bootstrap (200 resamples of the (budget, architecture) cells) gives a 95% CI of [0.41, 0.53] around the point estimate, with zero bootstrap samples reaching either  $\varphi = 0$  or  $\varphi = 1$ . The fit-quality difference is substantial: the constrained  $\varphi = 1$  fit drops  $R^2$  from 0.997 to 0.955, and the  $\varphi = 0$  restriction ( $r$  invisible to the law) reaches  $R^2 = 0.986$ . These  $R^2$  values are uniformly high because validation losses span only  $\sim 0.1$  nats across architectures, so seemingly small drops correspond to meaningful per-run residuals. Figure 1 (right) clearly visualizes the better fit. Further robustness checks are reported in Appendix E.

The joint-law compute-optimal frontier (Figure 1, right) trails the  $r=1$  baseline throughout the studied range and reproduces the gap pattern of the per-architecture analysis above: growing with compute budget and flattening at our largest. Reducing the fit from 20 parameters (four separate Chinchilla laws) to 6 (one joint law) costs only  $\sim 2 \times 10^{-3}$  in  $R^2$ . We read the joint law as a tighter summary of the same surface.

## 5 Downstream Evaluation

The scaling-law analysis summarises the sharing cost on validation loss with a single exponent  $\varphi$ , but not where that cost falls across downstream capabilities. We therefore re-evaluate every iso-FLOPs

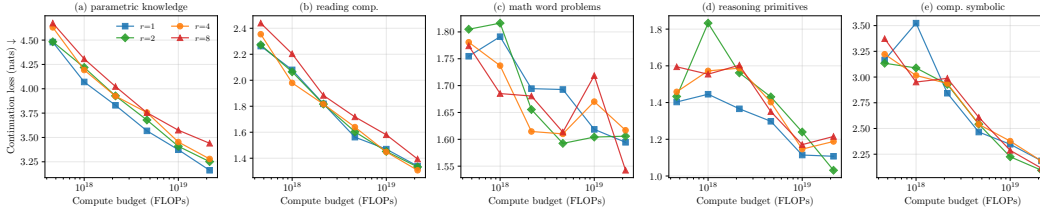


Figure 4: Compute-optimal downstream evaluation. Per-axis continuation loss at the  $r$ -specific checkpoint with lowest validation loss, per compute budget, for  $r \in \{1, 2, 4, 8\}$ . The five axes are defined in Appendix F. Lower is better.

checkpoint at each  $r \in \{1, 2, 4, 8\}$  on a five-axis downstream suite: *parametric knowledge* (closed-book QA), *reading comprehension* (in-context extraction), *math word problems* (multi-step arithmetic in natural language), *reasoning primitives* (induction-head and variable-assignment probes), and *compositional symbolic* (Dyck, ARC, BigBench algorithmic tasks). Per-task settings and rationale are in Appendix F. Following Heineman et al. [28], we report per-token continuation loss on the gold continuation as the primary signal (see Appendix F.4). We focus on the *compute-optimal* models: at each FLOPs budget we pick the checkpoint with the lowest validation loss.

The results in Figure 4 split the five axes into three regimes.

**Parametric knowledge tracks the validation-loss ordering.** Parametric knowledge is closed-book recall and therefore capacity-bound. The  $r=1$  baseline leads at every compute budget, and the gap grows monotonically with  $r$ , reaching 0.28 nats at  $r=8$ . This ordering matches the prediction from  $\varphi = 0.46$ : more recurrences share more parameters, leaving less unique-parameter capacity for knowledge storage.

**Reading comprehension and compositional symbolic close the gap.** Reading comprehension and compositional symbolic close the gap between architectures seen on parametric knowledge. On reading comprehension,  $r \in \{2, 4\}$  match  $r=1$  and only  $r=8$  trails (0.05–0.18 nats). On compositional symbolic, aggregates are roughly tied across  $r$  at all budgets, with mixed per-task outcomes (Appendix F.2). Looped variants lead on BigBench Dyck,  $r=1$  leads on QA-Wikidata and ARC-Easy, and CS-algorithms is essentially tied.

**Reasoning primitives and math word problems are unresolvable at our scale.** Reasoning primitives and math word problems are the axes on which depth-recurrent models are predicted to win most strongly [2, 29, 4], yet neither resolves a per- $r$  signal at our budgets. On reasoning primitives the  $r=1$  baseline leads at nearly every budget. On math word problems, continuation loss improves with overall model quality but per- $r$  separation falls inside noise. Both axes improve with validation loss in aggregate, but per- $r$  separation is below our resolution, so these axes cannot drive architectural decisions at our scale. Reasoning tasks are too challenging for small models to show signal.

## 6 Discussion

**The “worth” of a recurrence.** At matched depth, looped and non-looped transformers spend the same per-token forward-backward compute, but the looped model has only  $1/r$  of the unique blocks. The shared block must compensate by being applied to each token  $r$  times rather than once, lowering parameter count in exchange for more compute per parameter. Our fit shows this does not fully offset the parameter count. At  $r=4$  the shared block recovers  $4^{0.46} \approx 1.86$  unique blocks’ worth of capacity, about 47% of full equivalence ( $\varphi=1$ ). Each recurrence is thus worth less than a unique block.

However,  $\varphi$  is not fixed. It reflects our vanilla training setup, and several changes to the looped model could raise it by reducing training-FLOPs per recurrence, using the saved compute for a larger architecture or more training tokens. Potential methods include: shrinking the shared fraction (larger prelude/coda), truncated backpropagation [3], per-token early exit and adaptive compute [5, 6], retrofitting pretrained non-looped models [7, 8], and training with a diffusion objective in place of unrolling the loops [30]. All are compatible with our joint-law framework, and future work should

quantify  $\Delta\varphi$  for each. That said, no method is free: shrinking the shared fraction likely weakens the reasoning inductive bias, truncated BPTT can introduce training instabilities [3, 9], per-token exit breaks token-forward parallelism [5], and diffusion objectives push iteration cost from training to inference. We therefore study the vanilla prelude-recur-coda case and measure  $\varphi = 0.46$  as the baseline future recipes should beat, potentially to  $\varphi > 1$ , if the compute savings of these methods outweigh the parameter-sharing cost.

**Validation loss as the research target.** Section 5 splits the downstream surface into three regimes: parametric knowledge shows a clean capacity drop, reading comprehension and compositional symbolic track validation loss with similar performance across architectures, and the reasoning-heavy axes on which depth-recurrent models are predicted to win are compute-floored at our budgets. On the resolvable axes, per-axis continuation loss tracks validation loss in ordering. The axes where looped models are predicted to excel are precisely the axes our compute window cannot resolve, so the per-axis decomposition confirms rather than replaces validation loss as the signal that drives architectural decisions at development-scale compute. Closing the validation-loss gap is likely the most measurable target for looped LM research at these scales, and quantifying  $\Delta\varphi$  under any of the interventions above is a clean comparison between recipes.

**Designing fair comparisons.** Our results show that the compute-optimal allocation does not transfer across architectures (Section 4.2). Looped variants prefer wider widths and fewer training tokens than the non-looped baseline. Two consequences follow for anyone running matched-compute comparisons. First, a single  $(N, D)$  point cannot be compute-optimal for all architectures simultaneously. Either the width-budget is chosen for one variant and the others run off-optimum, or each architecture is trained at its own compute-optimum and the comparison crosses different  $(N, D)$ . Second, once widths differ, a compute-optimal looped model also uses more per-token inference FLOPs than its compute-optimal non-looped counterpart (an issue we flagged for iso-parameter scaling laws in Section 2). Thus, comparisons at matched *training* compute do not extend to matched *inference* compute. Extending the joint law with an inference-compute axis [31] is a natural next step.

**Limitations.** Our iso-depth grid spans  $\sim 50\times$  in training compute. Spot checks at larger training budgets would confirm that the ordering holds past our grid, and could test whether the reasoning axes show clearer separation. We also fix a single architecture configuration: 20 effective layers with  $(n_{\text{prelude}}, n_{\text{coda}}) = (2, 2)$  following the prelude-recur-coda template of Geiping et al. [3]. Different depth allocations or prelude/coda sizes may shift  $\varphi$ , and we leave this to future work.

## 7 Conclusion

We introduced an iso-depth scaling-law setup for looped language models that isolates parameter sharing from effective depth, and measured the *recurrence-equivalence exponent*  $\varphi = 0.46$ . A shared block looped  $r$  times is not equivalent to  $r$  unique blocks: each additional recurrence predictably *increases* validation loss at matched training compute. Downstream, the gap persists on parametric-knowledge tasks and closes on simple open-book tasks, while reasoning benefits of looped models are not resolvable at development-scale compute budgets, making the validation-loss gap the reliable target for looped LM research. Looped LMs remain attractive for their training and deployment flexibility, and directions such as relaxing full-BPTT, adaptive recurrence, and retrofitting offer concrete routes to raise  $\varphi$  and close the performance gap.

## References

- [1] Mostafa Dehghani, Stephan Gouws, Oriol Vinyals, Jakob Uszkoreit, and Łukasz Kaiser. Universal transformers. In *International Conference on Learning Representations (ICLR)*, 2019.
- [2] Nikunj Saunshi, Nishanth Dikkala, Zhiyuan Li, Sanjiv Kumar, and Sashank J. Reddi. Reasoning with Latent Thoughts: On the Power of Looped Transformers, February 2025.
- [3] Jonas Geiping, Sean McLeish, Neel Jain, John Kirchenbauer, Siddharth Singh, Brian R. Bartoldson, Bhavya Kailkhura, Abhinav Bhatele, and Tom Goldstein. Scaling up Test-Time Compute with Latent Reasoning: A Recurrent Depth Approach, February 2025.

- [4] Rui-Jie Zhu, Zixuan Wang, Kai Hua, Tianyu Zhang, Ziniu Li, Haoran Que, Boyi Wei, Zixin Wen, Fan Yin, He Xing, Lu Li, Jiajun Shi, Kaijing Ma, Shanda Li, Taylor Kergan, Andrew Smith, Xingwei Qu, Mude Hui, Bohong Wu, Qiyang Min, Hongzhi Huang, Xun Zhou, Wei Ye, Jiaheng Liu, Jian Yang, Yunfeng Shi, Chenghua Lin, Enduo Zhao, Tianle Cai, Ge Zhang, Wenhao Huang, Yoshua Bengio, and Jason Eshraghian. Scaling Latent Reasoning via Looped Language Models, November 2025.
- [5] Sangmin Bae, Yujin Kim, Reza Bayat, Sungnyun Kim, Jiyouon Ha, Tal Schuster, Adam Fisch, Hrayr Harutyunyan, Ziwei Ji, Aaron Courville, and Se-Young Yun. Mixture-of-Recursions: Learning Dynamic Recursive Depths for Adaptive Token-Level Computation, October 2025.
- [6] Tianyu Fu, Yichen You, Zekai Chen, Guohao Dai, Huazhong Yang, and Yu Wang. Think-at-Hard: Selective Latent Iterations to Improve Reasoning Language Models, November 2025.
- [7] Sean McLeish, Ang Li, John Kirchenbauer, Dayal Singh Kalra, Brian R. Bartoldson, Bhavya Kailkhura, Avi Schwarzschild, Jonas Geiping, Tom Goldstein, and Micah Goldblum. Teaching Pretrained Language Models to Think Deeper with Retrofitted Recurrence, November 2025.
- [8] Yeskendir Koishckenov, Aldo Lipani, and Nicola Cancedda. Encode, Think, Decode: Scaling test-time reasoning with recursive latent thoughts, October 2025.
- [9] Hayden Prairie, Zachary Novack, Taylor Berg-Kirkpatrick, and Daniel Y. Fu. Parcae: Scaling Laws For Stable Looped Language Models, April 2026.
- [10] Jordan Hoffmann, Sebastian Borgeaud, Arthur Mensch, Elena Buchatskaya, Trevor Cai, Eliza Rutherford, Diego de Las Casas, Lisa Anne Hendricks, Johannes Welbl, Aidan Clark, Tom Hennigan, Eric Noland, Katie Millican, George van den Driessche, Bogdan Damoc, Aurelia Guy, Simon Osindero, Karen Simonyan, Erich Elsen, Oriol Vinyals, Jack W. Rae, and Laurent Sifre. Training compute-optimal large language models. In *Proceedings of the 36th International Conference on Neural Information Processing Systems*, NIPS '22, Red Hook, NY, USA, 2022. Curran Associates Inc. ISBN 9781713871088.
- [11] Jared Kaplan, Sam McCandlish, Tom Henighan, Tom B. Brown, Benjamin Chess, Rewon Child, Scott Gray, Alec Radford, Jeffrey Wu, and Dario Amodei. Scaling Laws for Neural Language Models, January 2020.
- [12] Andrej Karpathy. nanochat: The best ChatGPT that \$100 can buy, 2025. URL <https://github.com/karpathy/nanochat>.
- [13] Biao Zhang and Rico Sennrich. Root mean square layer normalization. In *Advances in Neural Information Processing Systems (NeurIPS)*, 2019.
- [14] Jianlin Su, Yu Lu, Shengfeng Pan, Ahmed Murtadha, Bo Wen, and Yunfeng Liu. RoFormer: Enhanced transformer with rotary position embedding. *Neurocomputing*, 568, 2024.
- [15] Mostafa Dehghani, Josip Djolonga, Basil Mustafa, et al. Scaling vision transformers to 22 billion parameters. *International Conference on Machine Learning (ICML)*, 2023.
- [16] David R. So, Wojciech Mańke, Hanxiao Liu, Zihang Dai, Noam Shazeer, and Quoc V. Le. Primer: searching for efficient transformers for language modeling. In *Proceedings of the 35th International Conference on Neural Information Processing Systems*, NIPS '21, Red Hook, NY, USA, 2021. Curran Associates Inc. ISBN 9781713845393.
- [17] Tri Dao. Flashattention-2: Faster attention with better parallelism and work partitioning. In *The Twelfth International Conference on Learning Representations*, 2024. URL <https://openreview.net/forum?id=mZn2Xyh9Ec>.
- [18] Jay Shah, Ganesh Bikshandi, Ying Zhang, Vijay Thakkar, Pradeep Ramani, and Tri Dao. Flashattention-3: fast and accurate attention with asynchrony and low-precision. In *Proceedings of the 38th International Conference on Neural Information Processing Systems*, NIPS '24, Red Hook, NY, USA, 2024. Curran Associates Inc. ISBN 9798331314385.
- [19] Kaiyue Wen, Cheng Lu, et al. Training neural networks on the hyperball with the muon optimizer. *arXiv preprint arXiv:2602.02156*, 2025.

- [20] Keller Jordan. Muon: An optimizer for hidden layers in neural networks, 2024. URL <https://kellerjordan.github.io/posts/muon/>.
- [21] Ilya Loshchilov and Frank Hutter. Decoupled weight decay regularization. In *International Conference on Learning Representations (ICLR)*, 2019.
- [22] Liliang Ren, Yang Liu, Yelong Shen, and Weizhu Chen. Rethinking Language Model Scaling under Transferable Hypersphere Optimization, March 2026.
- [23] Anton Lozhkov, Loubna Ben Allal, Leandro von Werra, and Thomas Wolf. Fineweb-edu: the finest collection of educational content, 2024. URL <https://huggingface.co/datasets/HuggingFaceFW/fineweb-edu>.
- [24] Hugo Touvron, Louis Martin, Kevin Stone, Peter Albert, Amjad Almahairi, Yasmine Babaei, Nikolay Bashlykov, Soumya Batra, Prajjwal Bhargava, Shruti Bhosale, et al. Llama 2: Open foundation and fine-tuned chat models. *arXiv preprint arXiv:2307.09288*, 2023.
- [25] Peter J. Huber. Robust estimation of a location parameter. *The Annals of Mathematical Statistics*, 35(1):73–101, 1964. doi: 10.1214/aoms/1177703732.
- [26] Jorge Nocedal. Updating quasi-Newton matrices with limited storage. *Mathematics of Computation*, 35(151):773–782, 1980. doi: 10.1090/S0025-5718-1980-0572855-7.
- [27] Tamay Besiroglu, Ege Erdil, Matthew Barnett, and Josh You. Chinchilla scaling: A replication attempt. *arXiv preprint arXiv:2404.10102*, 2024.
- [28] David Heineman, Valentin Hofmann, Ian Magnusson, Yuling Gu, Noah A. Smith, Hannaneh Hajishirzi, Kyle Lo, and Jesse Dodge. Signal and Noise: A Framework for Reducing Uncertainty in Language Model Evaluation, August 2025.
- [29] Nikunj Saunshi, Nishanth Dikkala, Zhiyuan Li, Sanjiv Kumar, and Sashank J. Reddi. On the inductive bias of stacking towards improving reasoning. *arXiv preprint arXiv:2409.19044*, 2024.
- [30] Makoto Shing, Masanori Koyama, and Takuya Akiba. DiffusionBlocks: Block-wise Neural Network Training via Diffusion Interpretation, February 2026.
- [31] Nikhil Sardana, Jacob Portes, Sasha Dobov, and Jonathan Frankle. Beyond chinchilla-optimal: accounting for inference in language model scaling laws. In *Proceedings of the 41st International Conference on Machine Learning, ICML’24*. JMLR.org, 2024.
- [32] Johan Björck et al. Scaling laws under a more careful look at learning rate. *arXiv preprint arXiv:2510.24824*, 2025.
- [33] Angeliki Fan, Alex Graves, and Adhiguna Kuncoro. Looped transformers as programmable computers. *arXiv preprint arXiv:2301.13196*, 2024.
- [34] Gemma Team. Gemma 2: Improving open language models at a practical size, 2024. URL <https://arxiv.org/abs/2408.00118>.
- [35] Kaiming He, Xiangyu Zhang, Shaoqing Ren, and Jian Sun. Delving deep into rectifiers: Surpassing human-level performance on imagenet classification. In *2015 IEEE International Conference on Computer Vision (ICCV)*, pages 1026–1034, 2015. doi: 10.1109/ICCV.2015.123.
- [36] Jeffrey Li, Alex Fang, Georgios Smyrnis, et al. DataComp-LM: In search of the next generation of training sets for language models. *Advances in Neural Information Processing Systems (NeurIPS)*, 2024. Introduces the CORE benchmark and DCLM dataset.
- [37] Mandar Joshi, Eunsol Choi, Daniel S. Weld, and Luke Zettlemoyer. TriviaQA: A large scale distantly supervised challenge dataset for reading comprehension. *arXiv preprint arXiv:1705.03551*, 2017.

- [38] Tom Kwiatkowski, Jennimaria Palomaki, Olivia Redfield, Michael Collins, Ankur Parikh, Chris Alberti, Danielle Epstein, Illia Polosukhin, Jacob Devlin, Kenton Lee, Kristina Toutanova, Llion Jones, Matthew Kelcey, Ming-Wei Chang, Andrew M. Dai, Jakob Uszkoreit, Quoc Le, and Slav Petrov. Natural questions: A benchmark for question answering research. *Transactions of the Association for Computational Linguistics*, 7:452–466, 2019. doi: 10.1162/tacl\_a\_00276.
- [39] Jonathan Berant, Andrew Chou, Roy Frostig, and Percy Liang. Semantic parsing on Freebase from question-answer pairs. In *Proceedings of the 2013 Conference on Empirical Methods in Natural Language Processing*, pages 1533–1544, 2013.
- [40] Denis Paperno, Germán Kruszewski, Angeliki Lazaridou, Ngoc Quan Pham, Raffaella Bernardi, Sandro Pezzelle, Marco Baroni, Gemma Boleda, and Raquel Fernández. The LAMBADA dataset: Word prediction requiring a broad discourse context. In *Proceedings of the 54th Annual Meeting of the Association for Computational Linguistics (Volume 1: Long Papers)*, pages 1525–1534, 2016.
- [41] Jonathan H. Clark, Eunsol Choi, Michael Collins, Dan Garrette, Tom Kwiatkowski, Vitaly Nikolaev, and Jennimaria Palomaki. TyDi QA: A benchmark for information-seeking question answering in typologically diverse languages. *Transactions of the Association for Computational Linguistics*, 8:454–470, 2020. doi: 10.1162/tacl\_a\_00317.
- [42] Pranav Rajpurkar, Robin Jia, and Percy Liang. Know what you don’t know: Unanswerable questions for SQuAD. In *Proceedings of the 56th Annual Meeting of the Association for Computational Linguistics (Volume 2: Short Papers)*, pages 784–789, 2018. doi: 10.18653/v1/P18-2124.
- [43] Dheeru Dua, Yizhong Wang, Pradeep Dasigi, Gabriel Stanovsky, Sameer Singh, and Matt Gardner. DROP: A reading comprehension benchmark requiring discrete reasoning over paragraphs. In *Proceedings of the 2019 Conference of the North American Chapter of the Association for Computational Linguistics: Human Language Technologies*, pages 2368–2378, 2019. doi: 10.18653/v1/N19-1246.
- [44] Siva Reddy, Danqi Chen, and Christopher D. Manning. CoQA: A conversational question answering challenge. *Transactions of the Association for Computational Linguistics*, 7:249–266, 2019. doi: 10.1162/tacl\_a\_00266.
- [45] Arkil Patel, Satwik Bhattamishra, and Navin Goyal. Are NLP models really able to solve simple math word problems? In *Proceedings of the 2021 Conference of the North American Chapter of the Association for Computational Linguistics: Human Language Technologies*, pages 2080–2094, 2021. doi: 10.18653/v1/2021.naacl-main.168.
- [46] Shen-yun Miao, Chao-Chun Liang, and Keh-Yih Su. A diverse corpus for evaluating and developing English math word problem solvers. In *Proceedings of the 58th Annual Meeting of the Association for Computational Linguistics*, pages 975–984, 2020. doi: 10.18653/v1/2020.acl-main.92.
- [47] Rik Koncel-Kedziorski, Subhro Roy, Aida Amini, Nate Kushman, and Hannaneh Hajishirzi. MAWPS: A math word problem repository. In *Proceedings of the 2016 Conference of the North American Chapter of the Association for Computational Linguistics: Human Language Technologies*, pages 1152–1157, 2016. doi: 10.18653/v1/N16-1136.
- [48] Catherine Olsson, Nelson Elhage, Neel Nanda, Nicholas Joseph, Nova DasSarma, Tom Henighan, Ben Mann, Amanda Askell, Yuntao Bai, Anna Chen, Tom Conerly, Dawn Drain, Deep Ganguli, Zac Hatfield-Dodds, Danny Hernandez, Scott Johnston, Andy Jones, Jackson Kernion, Liane Lovitt, Kamal Ndousse, Dario Amodei, Tom Brown, Jack Clark, Jared Kaplan, Sam McCandlish, and Chris Olah. In-context learning and induction heads. *Transformer Circuits Thread*, 2022.
- [49] Aarohi Srivastava, Abhinav Rastogi, Abhishek Rao, Abu Awal Md Shoeb, Abubakar Abid, Adam Fisch, Adam R Brown, Adam Santoro, Aditya Gupta, Adrià Garriga-Alonso, et al. Beyond the imitation game: Quantifying and extrapolating the capabilities of language models. *arXiv preprint arXiv:2206.04615*, 2022.

[50] Peter Clark, Isaac Cowhey, Oren Etzioni, Tushar Khot, Ashish Sabharwal, Carissa Schoenick, and Oyvind Tafjord. Think you have solved question answering? try ARC, the AI2 reasoning challenge. *arXiv preprint arXiv:1803.05457*, 2018.

## A Extended Related Work

In this section, we expand the main-text Related Work (Section 2).

**Scaling laws.** Kaplan et al. [11] established power-law relations between loss, model size, and training tokens. Hoffmann et al. [10] refined the allocation (Chinchilla) and found that compute-optimal training scales parameters and tokens at roughly equal rates with compute. Subsequent work has examined learning-rate transfer [32, 22] and inference-aware scaling that trades training tokens for inference cost [31]. We extend these analyses to looped architectures.

**Iso-parameter scaling law.** Concurrent work by Prairie et al. [9] fits an iso-parameter scaling law at fixed unique parameter count  $N$ , with depth, per-token inference FLOPs, and KV cache memory all growing with the recurrence count  $\mu_{\text{rec}}$ . Their  $\mu_{\text{rec}}$  plays the role of our  $r$ , but is the *mean* of a distribution from which the per-step recurrence count is sampled during training, rather than a fixed architectural setting. At the core of their framework is the effective-parameter accounting  $N_{\text{eff}} = \mu_{\text{rec}}N$ : recurrences multiply the full unique parameter count, prelude and coda included. In our  $(N_{\text{once}} + r^\varphi N_{\text{rec}})$  decomposition, this accounting would scale  $N_{\text{once}}$  with  $r$  too, implying per-recurrence equivalence even stronger than  $\varphi = 1$ . On our iso-depth data, even the weaker  $\varphi = 1$  restriction already loses 0.042 in  $R^2$  (see Table 2).

Two further methodological details affect direct numerical comparison. (1) Prairie et al. [9] use truncated backpropagation through time (BPTT) throughout, with gradient window  $\mu_{\text{bwd}} = \lceil \mu_{\text{rec}}/2 \rceil$ , so at  $\mu_{\text{rec}}=8$  only the last 4 recurrences receive gradients. This reduces per-step training FLOPs on the recurrent block from  $\sim 6\mu_{\text{rec}}N_{\text{block}}D$  (full BPTT) to  $\sim 4\mu_{\text{rec}}N_{\text{block}}D$ , which at iso-compute translates to roughly 50% more training tokens at the same  $\mu_{\text{rec}}$ . Their parametric law has no  $\mu_{\text{bwd}}$  term and therefore includes the halving choice implicitly. We train under full backpropagation to keep training and inference FLOPs aligned with the matched non-looped baseline. (2) Prairie et al. [9]’s default input injection is diagonal ( $\mathcal{O}(d)$  parameters), so its per-token FLOPs contribution is negligible. Our injection is a linear map  $W_{\text{inject}} \in \mathbb{R}^{d \times 2d}$  and contributes a small but explicit cost (see Section 3.2). Both differences fall on the training-FLOPs axis discussed in Section 6. At iso-compute, a reduction in training FLOPs converts directly to a larger allocation of  $N$  and  $D$ , lowering val loss.

Overall, the two scaling laws are complementary and answer different questions. The methodological details, however, are transferable, and future work could test whether adopting them raises our  $\varphi$ .

**Per-token adaptive compute.** Adaptive per-token compute is one of the main promises of looped transformers. Not all tokens are equally hard to predict: common words follow from short context, while rare or reasoning-heavy tokens benefit from more computation. Fixed-depth transformers give every token the same compute budget, whereas a looped model, reusing a shared block, can in principle vary the recurrence count per token at no parameter cost. *Per-token early exit* realises this idea: loop on hard tokens, exit early on easy ones [1, 4, 3]. However, in practice, this method has not delivered wall-clock speedups in standard inference setups: parallel prefill and batched decoding assume all tokens to run the same number of layers per step, and variable-depth routing breaks this uniformity. Also KV cache entries are missing for some loops. Fixed per-token routing, as in Mixture-of-Recursions [5], can restore batching but introduces causality issues during routing.

**Test-time recurrence extrapolation.** The optimistic picture inherited from synthetic algorithmic tasks [33], of train short and deploy deep, has not transferred cleanly to general language modelling. Geiping et al. [3], Prairie et al. [9] train their models with Poisson-Lognormal-sampled recurrence counts extending to large values, to enable test-time scaling. However, Prairie et al. [9] fit a unified training-plus-inference law whose test-time component is a saturating exponential  $\mathcal{L}(T) = \mathcal{L}_\infty + Z \exp(-zT/\mu_{\text{rec}})$  that plateaus at  $T \approx \mu_{\text{rec}}$ . Thus, the training mean recurrence caps the test-time frontier, even though recurrence count is stochastically sampled during training. Zhu et al. [4]’s Ouro was trained with an entropy-regularised adaptive gate at maximum recurrence  $T_m=4$  and reports no inference-time gains beyond the trained depth. Taken together, effective inference depth in trained looped LMs concentrates near the training-exposed depth distribution rather than extrapolating freely past it. We therefore treat  $r$  as an architectural, not a test-time, scaling axis.

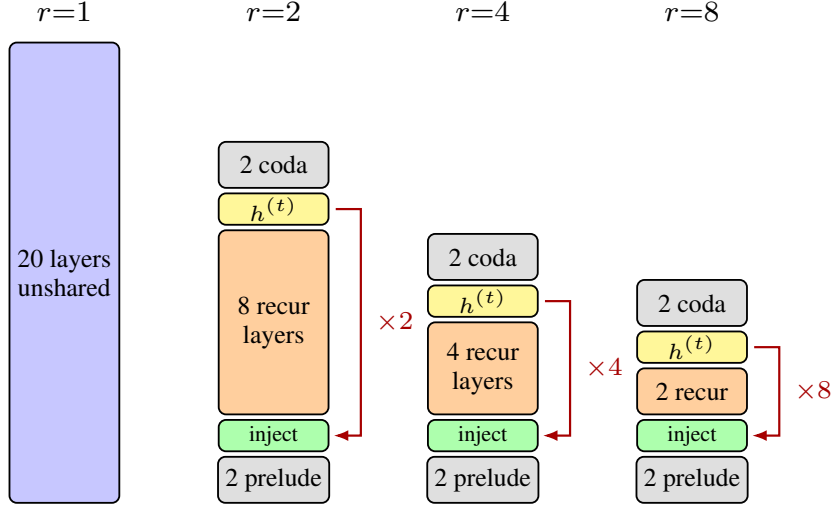


Figure 5: Architecture schematic for  $r \in \{1, 2, 4, 8\}$  at shared effective depth 20. The recurrent block (orange) is applied  $r$  times per forward pass and writes its output back into the latent state  $h^{(t)}$  (yellow) via the injection layer (green). Prelude and coda (grey) are unshared.

Table 3: Transformer architecture.

Component	Details
Sequence length	$T = 2048$ tokens
Attention	Full causal self-attention, no sliding window, no dropout
Attention backend	FlashAttention-2 [17] on A100, FlashAttention-3 [18] on H100
Position encoding	Rotary embeddings [14], base $\theta = 10,000$
Head dimension	$d_{\text{head}} = 128, n_{\text{head}} = d_{\text{model}}/128$
QK normalisation	Functional RMSNorm on $q, k$ before attention [15]
MLP activation	Squared ReLU [16], hidden dim = $4d_{\text{model}}$
Normalisation	Learnable RMSNorm [13], pre-norm, $\epsilon=10^{-6}$
Biases	None (all linear layers bias-free)
Embeddings	Untied wte and lm_head, token embeddings cast to bf16
Vocabulary	Llama 2 tokenizer [24], padded 32008 $\rightarrow$ 32064 for tensor-core alignment
Logit softcap	$z = 15 \cdot \tanh(\text{logits}/15)$ [34], applied in fp32 before the loss
Dropout	None

## B Model Architecture

### B.1 Implementation Details

All architectures are decoder-only transformers built on top of nanochat [12], using the same pre-norm block summarised in Table 3. The layer partition for each  $r$  is  $n_{\text{prelude}} + r \cdot n_{\text{recur}} + n_{\text{coda}} = 20$  with  $(n_{\text{prelude}}, n_{\text{coda}}) = (2, 2)$  for  $r > 1$  and  $(0, 0)$  for  $r=1$ , so  $n_{\text{recur}} = 16/r$  evaluates to  $\{8, 4, 2\}$  for  $r \in \{2, 4, 8\}$ . Figure 5 visualises the four stacks.

Each transformer block computes

$$\hat{x} = x + \text{Attn}(\text{RMSNorm}(x)), \quad x_{\text{out}} = \hat{x} + \text{MLP}(\text{RMSNorm}(\hat{x})).$$

In addition to the pre-norms inside each block, three model-level RMSNorms are applied on the residual stream: one after the token embedding, one at the end of every recurrence iteration (so the state handed to the next iteration or to the coda has controlled scale), and one before the lm\_head.

**Input injection (looped only).** For each looped architecture ( $r > 1$ ), every recurrence iteration begins with a linear injection step

$$u^{(t)} = W_{\text{inject}} [e \parallel h^{(t)}], \quad W_{\text{inject}} \in \mathbb{R}^{d \times 2d}, \quad (9)$$

where  $e$  is the prelude output (constant across recurrences),  $h^{(t)}$  is the recurrent state at iteration  $t$  with  $h^{(0)} = e$ , and  $W_{\text{inject}}$  is initialised as  $[I \parallel 0]$  so that  $u^{(0)} \approx e$  at the start of training. Appendix B.2 ablates this choice against additive-residual and no-injection variants.

**Initialisation.** Token embeddings are drawn from  $\mathcal{N}(0, 1)$  and then cast to bf16; the LM head is  $\mathcal{N}(0, 10^{-3})$ . Attention and MLP weights use  $\mathcal{U}(-a, a)$  with  $a = \sqrt{3}/\sqrt{d_{\text{model}}}$  (equivalently, the same standard deviation  $1/\sqrt{d_{\text{model}}}$  as the matched normal but with bounded tails), except `mlp.c_proj` which uses  $a = \sqrt{3}/\sqrt{4d_{\text{model}}}$  (Kaiming fan-in [35] over its input width  $4d_{\text{model}}$ ). The injection layer is initialised as  $[I \parallel 0]$ , and all RMSNorm scales are initialised to one.

## B.2 Input-Injection Ablation

Our default injection is the linear map of Equation 9, following the concatenation-injection design of Geiping et al. [3]. The linear map adds  $2d_{\text{model}}^2$  parameters and, applied once per recurrence, a non-negligible FLOPs overhead that is paid back only if it improves quality. We verify this at the reference configuration ( $s=10$ ,  $r=4$ , target compute  $10^{18}$  FLOPs) against two parameter-free alternatives:

- **Passthrough** ( $u^{(t)} = h^{(t)}$ ): no injection, recurrence is depth-only with  $h^{(0)}$  initialised from the prelude output.
- **Additive** ( $u^{(t)} = h^{(t)} + e$ ): parameter-free residual injection with  $h^{(0)} = 0$ , so the first iteration sees  $u^{(0)} = e$ .

All three runs use the same target FLOPs budget, so the parameter-free variants train on *more* tokens than the linear injection (973M vs. 955M, a  $\sim 2\%$  data advantage from the saved injection FLOPs). Final validation losses are 2.793 nats for the linear injection, 2.797 for additive, and 7.400 for passthrough. Passthrough fails to train, showing that input injection is essential at this scale. Additive is competitive but trails the linear injection by 0.004 nats despite its  $\sim 2\%$  token advantage. We therefore adopt the linear injection for all reported scaling-law runs. Its FLOPs overhead is accounted for in  $n_{\text{recur}}$  in Equation 2 and thus included in every iso-FLOPs comparison.

## C Hyperparameter Tuning

### C.1 Learning Rate Sweep

We sweep the MuonH [22, 19] matrix learning rate at  $s=10$  with a tokens-per-parameter ratio of 10 ( $\sim 1\text{B}$  training tokens) and batch size  $B = 262,144$  (256K), independently for each architecture, using eight LR values per architecture in the range  $\eta \in [0.008, 0.024]$  with extra density around the optimum. The batch size was chosen from a separate sweep at the same reference configuration over  $B \in \{256\text{K}, 512\text{K}, 1\text{M}\}$  tokens, where 256K yielded uniformly lower loss for both architectures.

Both architectures converge to a shared optimum near  $\eta^* \approx 0.014$ , which we adopt as the base learning rate for all subsequent experiments (Figure 6). Both models’ loss landscape is flat near the optimum: LRs from 0.012 to 0.016 produce losses within 0.001 nats.

### C.2 Transfer Validation

Under the HyperP framework [22] the *base* learning rate  $\eta_{\text{base}}$  (the value fed into HyperP before its width and data corrections are applied) should be invariant to both width and training horizon (after the  $T^{-0.32}$  data-scaling correction of the HyperP LR rule). We verify both claims by repeating the LR sweep under varied conditions and measuring the regret: the loss penalty of using  $\eta_{\text{base}} = 0.014$  instead of the per-condition optimum.

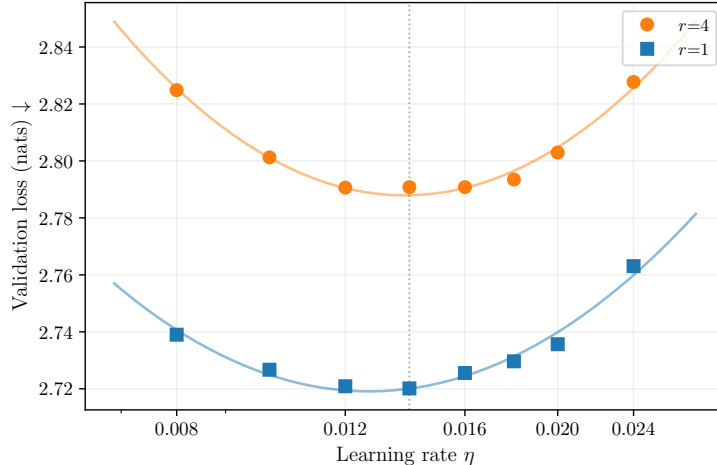


Figure 6: Learning rate sweep at  $s=10$  (ratio 10,  $B = 256\text{K}$ ). Both architectures exhibit a clear U-shaped loss landscape with a shared optimum near  $\eta^* \approx 0.014$ . The dotted vertical line marks  $\eta = 0.014$ , the base LR adopted for all scaling-law runs. The looped curve is notably flat: LRs from 0.012 to 0.016 are within 0.001 nats of the optimum.

Table 4: Iso-compute grid. Left: unique non-embedding parameter count  $N$  (M) per (width, recurrence) cell. Right: training tokens (B) per (width, budget) cell for  $r = 1$ .

$s$	Unique params $N$ (M)				Training tokens (B) per budget (FLOPs)					
	$r=1$	$r=2$	$r=4$	$r=8$	$4.64 \cdot 10^{17}$	$10^{18}$	$2.15 \cdot 10^{18}$	$4.64 \cdot 10^{18}$	$10^{19}$	$2.15 \cdot 10^{19}$
6	35.4	21.5	14.5	10.9	0.98	2.10	—	—	—	—
8	62.9	38.3	25.7	19.4	0.64	1.36	2.95	—	—	—
10	98.3	59.8	40.2	30.3	0.45	0.97	2.08	4.49	—	—
12	141.6	86.1	57.8	43.7	0.34	0.72	1.55	3.34	7.13	—
14	192.7	117.2	78.7	59.4	—	0.56	1.20	2.59	—	—
16	251.7	153.1	102.8	77.6	—	—	0.96	2.07	4.43	—
18	318.6	193.8	130.1	98.2	—	—	—	1.70	3.62	7.78
20	393.3	239.2	160.6	121.3	—	—	—	1.42	3.05	—
24	566.3	344.5	231.2	174.6	—	—	—	—	2.20	4.71
28	770.8	468.9	314.7	237.7	—	—	—	—	—	3.58
34	1136.5	691.4	464.1	350.4	—	—	—	—	—	2.52

**Width transfer.** We sweep at  $s \in \{8, 10, 14\}$  (ratio 10,  $B = 256\text{K}$ ). Figure 7 (left column) shows the regret U-curves in base LR space: all minima cluster near  $\eta_{\text{base}} = 0.014$  with a maximum regret of 0.004 nats ( $s=8$  looped). As a lightweight sanity check past the sweep range, we run the two candidate LRs  $\eta_{\text{base}} \in \{0.012, 0.014\}$  at  $s=18$  for the looped architecture and find 0.014 marginally better (2.473 vs. 2.476 nats), confirming that 0.014 remains near-optimal.

**Data scaling.** We sweep at  $s=10$  ( $B = 256\text{K}$ ) with ratios  $\{10, 20, 40\}$ , spanning a  $4\times$  range in training tokens. If the  $T^{-0.32}$  exponent is correct, the data-scaling correction adjusts the effective LR automatically and the optimal base LR should remain constant. Figure 7 (right column) confirms this: regret at  $\eta_{\text{base}} = 0.014$  stays below 0.005 nats across all ratios for both architectures.

## D Iso-Depth Grid

For each compute budget we sweep model width to find the compute-optimal point at every recurrence count  $r \in \{1, 2, 4, 8\}$ . Table 4 reports the unique non-embedding parameter count  $N(s, r)$  at each width and the training tokens  $D$  used at each (budget, width) cell. Looped models train on slightly less tokens due to input injection compute overhead. Empty cells are untested widths.

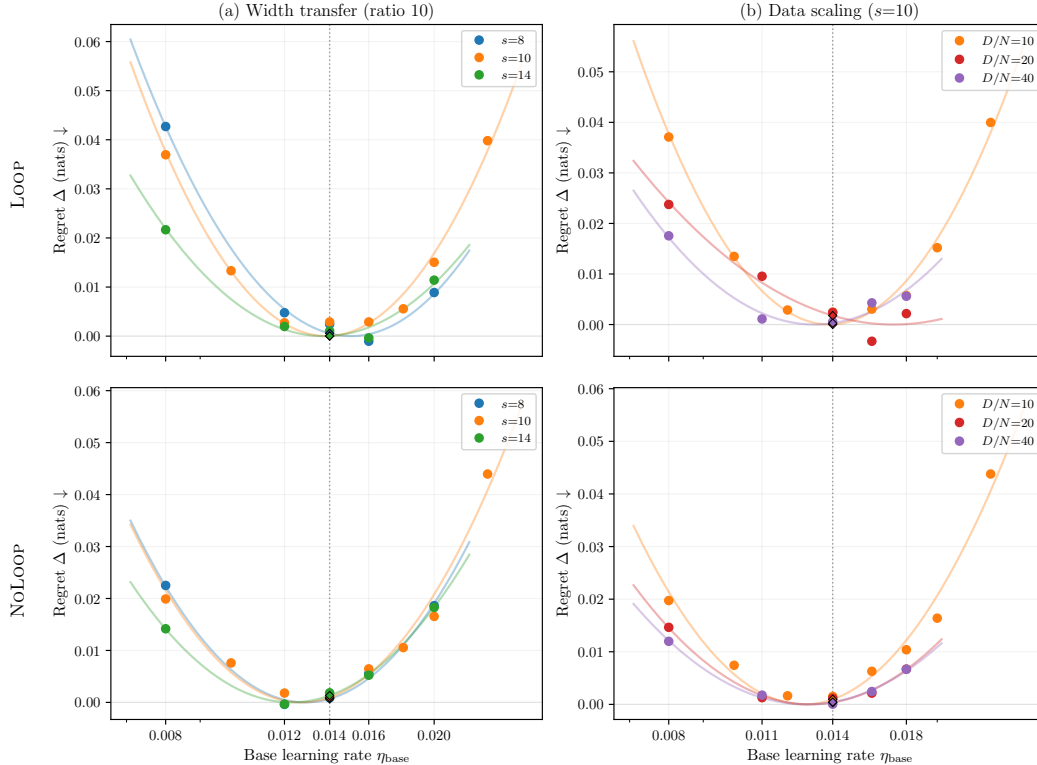


Figure 7: Transfer validation. Regret (loss above the per-condition optimum) vs. base learning rate  $\eta_{\text{base}}$ . Vertical dotted line marks  $\eta_{\text{base}} = 0.014$ ; diamond markers show the regret at that point. Rows split by architecture (looped  $r=4$ , top; non-looped  $r=1$ , bottom). All conditions incur  $\leq 0.005$  nats regret, so  $\eta_{\text{base}} = 0.014$  transfers cleanly across width and training horizon.

## E Scaling Law Fit Diagnostics

We conduct robustness checks for the per-architecture Chinchilla fits (Equation 7) and the joint  $(N_{\text{once}}, N_{\text{rec}}, D, r)$  law (Equation 6): residuals for the per-architecture fits, aggregate residual statistics for the joint fit, the block-bootstrap procedure behind the  $\varphi$  confidence interval, stability of  $\varphi$  across budget halves, and the shared- $E$  identifiability problem.

### E.1 Per-Architecture and Joint Fit Residuals

Figure 8 shows predicted vs. actual validation loss for the four per-architecture Chinchilla fits; points cluster tightly around the diagonal with a maximum residual below 0.007 nats. Figure 9 plots the same residuals against  $N$  and  $D$  and shows no systematic bias across either axis.

On the joint law, which fits all 116 runs with six shared parameters  $(A, \alpha, B, \beta, E, \varphi)$  rather than 20 per-architecture parameters, residuals are naturally larger:  $\max |\text{resid}| = 0.036$  nats and  $\text{RMSE} = 0.010$  nats. This is expected given the stronger constraint, and the joint fit still reaches  $R^2 = 0.997$ . Spearman rank-correlation tests of the joint residuals show no systematic structure:  $\rho_N = +0.04$  ( $p = 0.68$ ) against unique parameters and  $\rho_D = +0.05$  ( $p = 0.62$ ) against training tokens. We do not plot the joint-law residuals separately. The per-architecture panels in Figure 9 provide a stricter visual check on the same runs.

### E.2 Bootstrap Procedure

The 95% CI reported alongside the joint-law point estimate ( $\varphi = 0.46$ ,  $[0.41, 0.53]$ ) is a block bootstrap over  $(\text{budget}, \text{architecture})$  cells: each cell groups all widths trained at a given (compute budget,  $r$ ) pair, so resampling respects the experimental block structure rather than treating individual

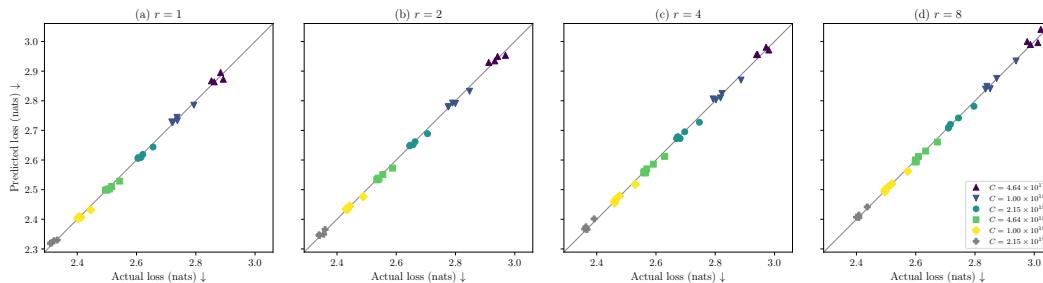


Figure 8: Per-architecture Chinchilla fit quality: predicted vs. actual validation loss, one panel per architecture ( $r \in \{1, 2, 4, 8\}$ ). Markers redundantly encode the compute budget by both shape and colour. Points cluster tightly around the identity line across all four architectures.

runs as independent. We draw 200 resamples with replacement of the non-empty cells (6 budgets  $\times$  4 architectures), refit the joint law on each resample, and report the 2.5th / 97.5th percentiles of the resulting  $\varphi$  distribution. Zero resamples reach either  $\varphi = 0$  or  $\varphi = 1$ . The shared- $E$  alternative below reports a point estimate only, we do not bootstrap it.

### E.3 Stability Across Budget Halves

Refitting the joint law separately on the low-budget half ( $C \leq 2.15 \times 10^{18}$ ,  $n=56$  runs) gives  $\varphi = 0.44$ , and refitting on the high-budget half ( $C \geq 4.64 \times 10^{18}$ ,  $n=60$  runs) gives  $\varphi = 0.49$ .  $\varphi$  therefore does not drift with scale inside our compute window, and the bootstrap CI comfortably contains both half-window estimates.

## F Downstream Evaluation Suite

### F.1 Setup

The downstream suite partitions tasks into five mechanistically motivated axes, each isolating a single capability dimension so that architectural biases can be read off directly. Tasks are sourced from the CORE benchmark [36], the Saunshi suite [2], and a small set of in-house probes. Per-task settings are in Table 5.

Few-shot counts were chosen to match or approximate the source benchmarks’ canonical settings. CoQA is reduced to 1-shot because the full-passage prompts frequently exceed the 2,048-token context used throughout pretraining. All four architectures share the same shot count and prompts on every task.

#### Axes and rationale.

- **Parametric knowledge.** Closed-book QA that requires recall of facts stored in weights, with no supporting passage. TriviaQA [37], NaturalQuestions [38], WebQuestions [39]. Probes unique-parameter capacity for factual storage.
- **Reading comprehension.** Extract or continue answer spans from an in-context passage. Lambada-OpenAI [40], TydiQA-GoldP [41], SQuADv2 [42], DROP [43], CoQA [44]. Probes in-context binding and multi-sentence extraction.
- **Math word problems.** Grade-school arithmetic in natural language: SVAMP [45], AS-Div [46], MAWPS [47]. Probes multi-step numeric chaining.
- **Reasoning primitives.** Minimal in-context symbolic operations. An induction-head probe following Olsson et al. [48] and four variable-assignment probes reimplemented from Saunshi et al. [29] (depth 0 and depth 1, each in math and code surface formats). *Variable assignment*: each example presents 5 direct integer assignments (depth 0) or 5 direct assignments plus 5 one-hop aliases with a 1-to-1 base-alias mapping (depth 1), in either a math format (“ $n=22$ ”) or a Python format (“ $n = 22$ ”), with English scaffolding. Values are drawn from [1, 25], and the answer is the queried variable’s integer value.

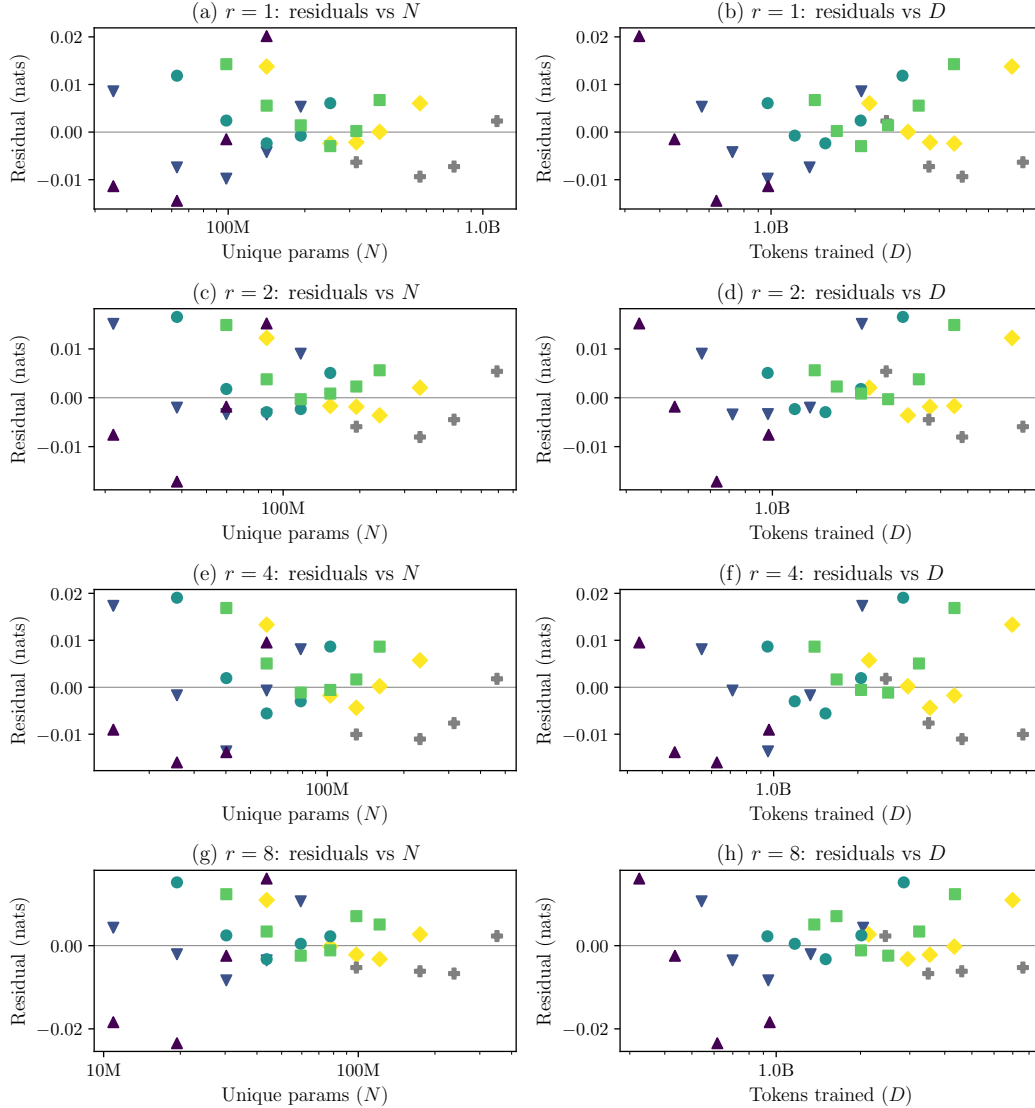


Figure 9: Per-architecture Chinchilla fit residuals (actual – predicted) vs. unique parameters  $N$  (left column) and tokens  $D$  (right column). Rows are the four architectures  $r \in \{1, 2, 4, 8\}$ . Markers encode the compute budget by both shape and colour.

- **Compositional symbolic.** Multi-step structured manipulation over in-context sequences: BigBench Dyck-languages [49], BigBench QA-Wikidata [49], ARC-Easy [50], BigBench CS-algorithms [49].

## F.2 Per-Task Continuation Loss

The five-axis aggregates in the main text average over multiple tasks. Table 6 reports the underlying per-task continuation loss at the per-architecture compute-optimal checkpoint at the largest training budget  $C = 2.15 \times 10^{19}$  FLOPs. The last column shows the dynamic range of  $r=1$  continuation loss across the six budgets at the  $r=1$  compute-optimal checkpoint of each budget, giving a sense of how much room each task improves with compute.

A few per-task patterns are consistent with the axis-level aggregates. On parametric knowledge,  $r=1$  has the lowest loss on all three tasks with a monotone ordering across  $r$ , reproducing the validation-loss ordering. The reading-comprehension ordering varies task by task: TydiQA-GoldP, SQuADv2,

Table 5: Per-task settings. Type: MC = multiple choice, LM = language modelling (continuation log-likelihood). Continuation loss is reported throughout. Samples is the number of examples actually scored: all tasks are capped at 10,000 examples (TriviaQA and BigBench QA-Wikidata, with 17,944 and 20,321 examples in the source datasets, are uniformly subsampled).

Axis	Task	Samples	Shots	Type
Parametric knowledge	TriviaQA [37]	10,000	5	LM
	NaturalQuestions [38]	3,610	5	LM
	WebQuestions [39]	2,032	5	LM
Reading comp.	Lambada-OpenAI [40]	5,153	0	LM
	TydiQA-GoldP [41]	440	3	LM
	SQuADv2 [42]	5,928	3	LM
	DROP [43]	9,535	3	LM
	CoQA [44]	7,983	1	LM
Math word problems	SVAMP [45]	300	5	LM
	ASDiv [46]	2,305	5	LM
	MAWPS [47]	1,772	5	LM
Reasoning primitives	Induction head (in-house)	1,000	0	LM
	VarAssign d0 (math) [29]	1,000	5	LM
	VarAssign d0 (code) [29]	1,000	5	LM
	VarAssign d1 (math) [29]	1,000	5	LM
	VarAssign d1 (code) [29]	1,000	5	LM
Compositional symbolic	BigBench Dyck [49]	1,000	10	LM
	BigBench QA-Wikidata [49]	10,000	10	LM
	ARC-Easy [50]	2,376	10	MC
	BigBench CS-algorithms [49]	1,320	10	LM

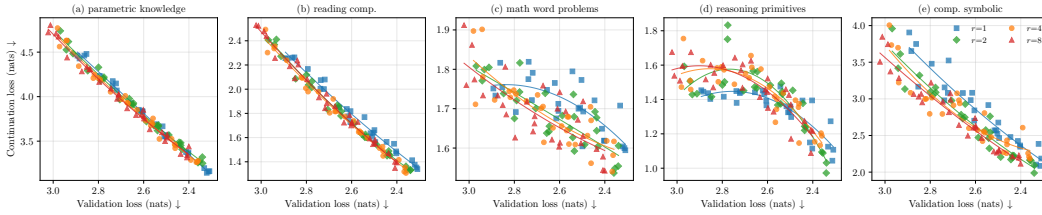


Figure 10: Per-axis continuation loss vs. validation loss for all iso-FLOPs checkpoints, coloured by recurrence count  $r \in \{1, 2, 4, 8\}$ . Curves are per- $r$  quadratic fits, and the x-axis is inverted (lower-loss models on the right).

DROP, and CoQA all favour  $r=4$ , while Lambada-OpenAI is monotone in  $r=1$ , consistent with the roughly flat reading-comp aggregate in Section 5. On compositional symbolic, the looped variants lead on BigBench Dyck, while on QA-Wikidata and ARC-Easy  $r=1$  leads, and BigBench CS-algorithms is essentially tied across  $r$ . On reasoning primitives, induction-head and var-assign d0 (math/code) carry most of the signal, with the d1 variants near random-guessing:  $r=2$  leads on induction-head and on var-assign d0 (code) and d1 (code),  $r=4$  on var-assign d0 (math), and  $r=1$  on d1 (math). Math word problems are compressed within  $\sim 0.1$  nats across  $r$ , so the small per-task differences should not be over-interpreted.

### F.3 Per-Axis Continuation Loss versus Validation Loss

Figure 10 complements the compute-optimal summary of Section 5 by plotting per-axis continuation loss against validation loss for every iso-Depth checkpoint. Each panel shows how one downstream axis tracks LM quality across the four architectures. Per- $r$  curves show a different ordering compared to the main figure because the architectures reach a given val loss with different  $(N, D)$  allocations.

Table 6: Per-task continuation loss (nats, lower is better) at the per-architecture compute-optimal checkpoint at  $C = 2.15 \times 10^{19}$  FLOPs. The last column shows the range of continuation loss across the six compute budgets at the  $r=1$  compute-optimal checkpoint of each budget.

Axis	Task	$r=1$	$r=2$	$r=4$	$r=8$	$r=1$ range over $C$
Parametric knowledge	TriviaQA	<b>3.251</b>	3.346	3.381	3.497	3.251–4.732
	NaturalQuestions	<b>3.158</b>	3.226	3.257	3.393	3.158–4.237
	WebQuestions	<b>3.079</b>	3.183	3.199	3.431	3.079–4.469
Reading comp.	Lambada-OpenAI	<b>1.910</b>	1.934	1.991	2.116	1.910–3.243
	TydiQA-GoldP	0.631	0.624	<b>0.564</b>	0.605	0.631–1.299
	SQuADv2	1.001	0.990	<b>0.924</b>	1.020	1.001–2.060
	DROP	1.674	1.667	<b>1.630</b>	1.736	1.674–2.096
	CoQA	1.482	1.449	<b>1.427</b>	1.492	1.482–2.616
Math word problems	SVAMP	1.645	1.634	1.643	<b>1.540</b>	1.631–1.778
	ASDiv	1.635	1.657	1.675	<b>1.634</b>	1.635–1.892
	MAWPS	1.503	1.526	1.532	<b>1.453</b>	1.503–1.703
Reasoning primitives	Induction head	1.760	<b>1.666</b>	2.208	2.187	1.760–2.339
	VarAssign d0 (math)	0.790	0.816	<b>0.715</b>	0.812	0.731–1.237
	VarAssign d0 (code)	0.891	<b>0.612</b>	0.787	0.815	0.823–1.162
	VarAssign d1 (math)	<b>0.986</b>	1.127	1.090	1.123	0.902–1.280
	VarAssign d1 (code)	1.110	<b>0.935</b>	1.142	1.141	0.990–1.232
Compositional symbolic	BigBench Dyck	3.902	3.419	3.733	<b>3.264</b>	3.902–6.943
	BigBench QA-Wikidata	<b>1.737</b>	1.808	1.874	1.999	1.737–3.544
	ARC-Easy	<b>1.977</b>	2.020	2.010	2.088	1.977–3.093
	BigBench CS-algorithms	1.127	1.127	1.117	<b>1.105</b>	1.123–1.286

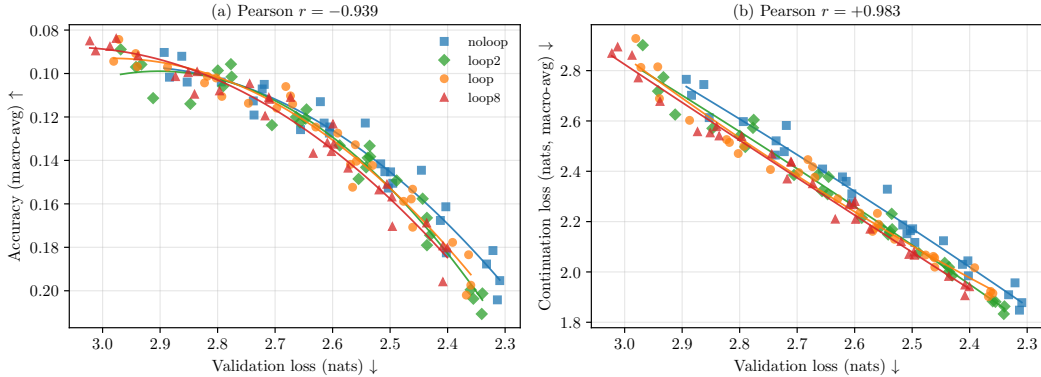


Figure 11: Macro-aggregate downstream metric vs. validation loss across iso-FLOPs checkpoints. Left: accuracy. Right: continuation loss. The x-axis is inverted so that lower-loss (more capable) models sit to the right. The accuracy y-axis is inverted so that “better” is downward on both panels.

#### F.4 Accuracy versus Continuation Loss

At small scales many tasks are near the random-chance accuracy floor, where accuracy is a coarse, bimodal signal. Following Heineman et al. [28] we report continuation loss throughout. Figure 11 shows the correlation of each metric with validation loss across all iso-FLOPs checkpoints: continuation loss tracks validation loss nearly linearly, while the accuracy aggregate is noisier and flat for small scales.